LETTERS

Molecular identification of a retinal cell type that responds to upward motion

In-Jung Kim[1]*, Yifeng Zhang[1]*, Masahito Yamagata[1], Markus Meister[1] & Joshua R. Sanes[1]

The retina contains complex circuits of neurons that extract salient information from visual inputs. Signals from photoreceptors are processed by retinal interneurons, integrated by retinal ganglion cells (RGCs) and sent to the brain by RGC axons. Distinct types of RGC respond to different visual features, such as increases or decreases in light intensity (ON and OFF cells, respectively), colour or moving objects[1–5]. Thus, RGCs comprise a set of parallel pathways from the eye to the brain. The identification of molecular markers for RGC subsets will facilitate attempts to correlate their structure with their function, assess their synaptic inputs and targets, and study their diversification. Here we show, by means of a transgenic marking method, that junctional adhesion molecule B (JAM-B) marks a previously unrecognized class of OFF RGCs in mice. These cells have asymmetric dendritic arbors aligned in a dorsal-to-ventral direction across the retina. Their receptive fields are also asymmetric and respond selectively to stimuli moving in a soma-to-dendrite direction; because the lens reverses the image of the world on the retina, these cells detect upward motion in the visual field. Thus, JAM-B identifies a unique population of RGCs in which structure corresponds remarkably to function.

Several adhesion molecules of the immunoglobulin superfamily (IgSF) are selectively expressed by RGC subsets in chick[6,7]. On the basis of these results, we surveyed the expression of about 200 IgSF genes in the mouse retina (see Methods). One such gene, *JAM-B*, was expressed by a small fraction of RGCs (Fig. 1a). Analysis of whole mounts showed that the *JAM-B*-positive RGCs were spaced relatively evenly across the retina (Fig. 1b, c), a 'mosaic' arrangement characteristic of many retinal cell types that share specific physiological or molecular properties[1,2,8]. JAM-B has been implicated in tight junction assembly and interactions of haematopoietic cells, but expression by neurons has not been reported[9].

To mark these cells for structural and functional study, we generated mice that express a ligand–activated Cre recombinase-oestrogen receptor fusion protein[10] (CreER) under the control of regulatory elements from the *JAM-B* gene (JAM-B–CreER; Fig. 1d). The rationale was as follows: *JAM-B* is expressed at low levels, so that linking *JAM-B* regulatory sequences directly to a reporter might result in inadequate marking. Linking *JAM-B* regulatory elements to Cre recombinase can amplify the signal: such mice can be mated to a line[11] in which Cre-mediated excision of a 'stop' cassette activates the strong expression of yellow fluorescent protein (Thy1-STOP–YFP). However, *JAM-B* is expressed in dynamic patterns in embryos, so in this scheme YFP would mark cells that expressed *JAM-B* transiently during development. The use of CreER circumvents this limitation, because it is only active for a short period after application of its activating ligand, tamoxifen[10]. A few hundred RGCs per retina were marked in JAM-B–CreER;Thy1-STOP–YFP mice after tamoxifen injection (Fig. 1e–h). Among the YFP-positive RGCs, at least 90% of the YFP-positive RGCs expressed *JAM-B* (Supplementary Fig. 1). We refer to the YFP-positive RGCs as J-RGCs.

Analysis of J-RGCs revealed three notable structural features. First, their dendrites were restricted to a narrow band within the outer third of the IPL (Fig. 1e and Supplementary Fig. 2a). The IPL is divided into at least ten sublaminae, and physiological properties of RGCs are related to the sublaminae in which their dendrites arborize[1,2,12]. Dendrites of J-RGCs arborized in a narrow band between processes of dopaminergic and cholinergic amacrines[13], indicating a sublaminar restriction (Fig. 1f) and suggesting that J-RGCs receive few synapses from these two amacrine classes. In contrast, processes of CD15-positive and AII amacrines did overlap with dendrites of J-RGCs (Supplementary Fig. 3) and may therefore provide input to them.

Second, about 85% of J-RGCs had markedly asymmetric dendritic arbors (Fig. 1g). One or two primary dendrites emerged from the soma and branched repeatedly at acute angles to fill a narrow sector; more than 90% of the dendritic field area lay on one side of the soma. In contrast, the vast majority of RGCs have dendrites that radiate far more symmetrically about the soma[14–16].

Third, and most remarkably, dendrites of asymmetric J-RGCs pointed in the same direction, slightly (about 13°) nasal of ventral (Fig. 1h, i). The dendritic orientation was longitudinal, from the dorsal to the ventral pole of the eye, instead of radial relative to the optic nerve head; this was most apparent after the correction of flat mounts for retinal curvature. The roughly 15% of J-RGCs that were not markedly asymmetrical were located near the dorsal and ventral margins of the retina (Fig. 1i). Therefore nearly all J-RGCs in central, nasal and temporal retina were asymmetric. Symmetric and asymmetric J-RGCs alike had dendrites confined to the outer part of the IPL (Supplementary Fig. 2).

The morphology of J-RGCs led to two hypotheses about their function. First, studies combining electrical recording with dye-filling have revealed that RGCs with dendrites in the outer third of the IPL are excited predominantly by dimming of light in the receptive field centre (OFF-RGCs)[1–3,12], suggesting that J-RGCs are OFF cells. Second, the dendritic asymmetry raised the possibility that J-RGCs are sensitive to stimuli with a particular orientation or direction. To test these ideas, we identified J-RGCs in retinal explants with fluorescence optics and recorded their visual responses.

When probed with small flashing spots near the cell soma, almost all J-RGCs fired when the light turned off (Fig. 2a). By contrast, recordings from non-fluorescent RGCs in the same retinae yielded, as expected[3], similar numbers of ON and OFF cells (Fig. 2b). Consistent with these physiological observations, processes of several classes of OFF bipolar cells[17,18] were present in the same sublamina as J-RGC dendrites, whereas processes of ON bipolars overlapped only minimally with J-RGC dendrites (Fig. 1f and Supplementary Fig. 3).

[1]Department of Molecular and Cellular Biology and Center for Brain Science, Harvard University, Cambridge, Massachusetts 02138, USA.
*These authors contributed equally to this work.

Thus, J-RGCs are likely to receive inputs from OFF but not ON bipolar cells. Interestingly, J-RGCs failed to fire in response to somewhat larger spots, and responded at light onset when they were larger still (Fig. 2c, d). Thus, the receptive field of J-RGCs is unusual[19] in that the integrated strength of its ON surround exceeds that of the OFF centre.

To probe the sensitivity of J-RGCs to motion, we moved a small spot through the receptive field centre in eight straight trajectories. The firing rate varied strongly with direction of motion (Fig. 2e and Supplementary Fig. 5). The preferred direction corresponded to the direction in which the dendritic tree pointed from the cell soma (Fig. 2f). Thus, in contrast to previously studied direction-selective RGCs, whose shape provides no clue to their physiological selectivity[2,4,5], the direction selectivity of J-RGCs is correlated with structural asymmetry.

To gain further insight into mechanisms underlying the direction-selectivity of J-RGCs, we measured their spatio-temporal receptive field by reverse correlation with randomly flickering bars (Fig. 3a, b).

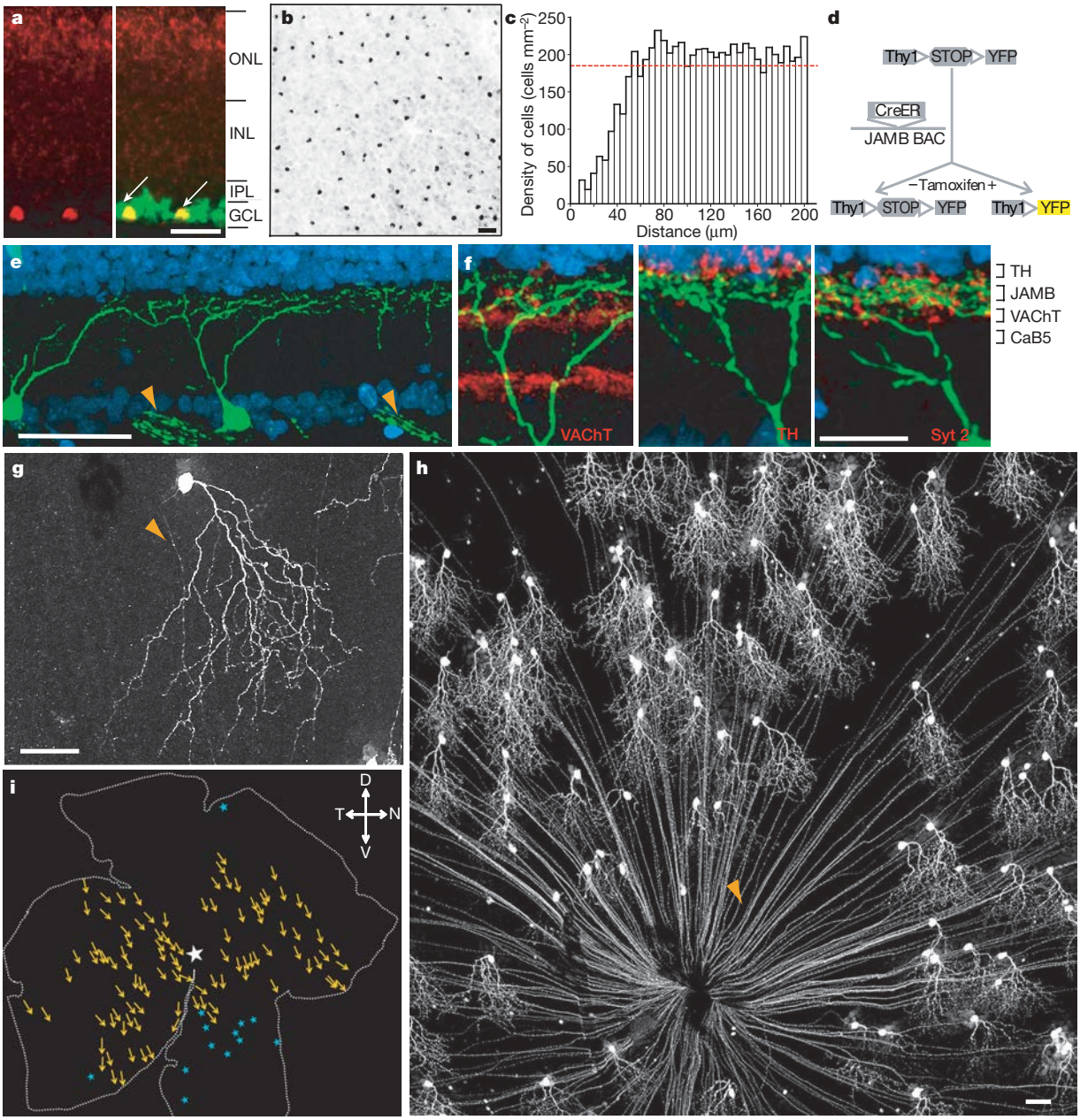

Figure 1 | JAM-B marks a structurally unique subset of RGCs. **a**, *In situ* hybridization of sections from P7 retina with probes to *JAM-B* (red) and *Thy1*, a pan-RGCs marker[29] (green). Left, *JAM-B* alone; right, merge. *JAM-B*-positive cells are RGCs (arrows). ONL, outer nuclear layer; INL, inner nuclear layer; IPL, inner plexiform layer; GCL, ganglion cell layer. **b**, Regular spacing of *JAM-B*-expressing RGCs revealed by *in situ* hybridization in a whole mount. **c**, Density recovery profile analysis[8] of retinae such as that shown in **b**. The dotted line shows expectation for random distribution at the same overall density. **d**, Transgenic system for marking J-RGCs with YFP. CreER, tamoxifen-activated Cre; open triangles, loxP sites. **e**, J-RGCs labelled with YFP (green) in sections from a JAM-B–CreER;Thy1-STOP–YFP double transgenic mouse. Blue, fluorescent Nissl stain. Dendrites of J-RGCs arborize in the outer part of the IPL. Arrowheads, axon bundles. **f**, Double staining of sections such as that in **e** shows that dendrites of J-RGCs arborize in a sublamina between those occupied by processes of amacrine cells positive for vesicular acetylcholine transporter (VAChT) and tyrosine hydroxylase (TH). Processes of bipolar cells positive for synaptotagmin-2 (Syt2) overlap with J-RGC dendrites. CaB5, calcium-binding protein 5. **g**, Asymmetric J-RGC from a whole mount. **h**, Micrograph of a whole-mounted retina. Arrowhead in **g** and **h** marks RGC axons. **i**, Sketch of another retina, showing orientation of J-RGC dendrites (arrows). Blue stars show cells with symmetric dendrites at the dorsal and ventral margins. White star, optic nerve head. D, dorsal; V, ventral; N, nasal; T, temporal. Scale bar, 50 μm (**a**, **b**, **e**, **g**–**i**) and 20 μm (**f**).

With the help of a 'linear–nonlinear' model[20], this receptive field was used to predict the cell's response to moving spots. The predicted direction selectivity matched the measurements (Supplementary Fig. 4), motivating further analysis of the receptive field for features that shape direction selectivity.

First, the ON-surround is markedly asymmetric, shifted in the preferred direction relative to the centre (Fig. 3d, e). In addition, the receptive field centre has a strongly biphasic time course: a distinct OFF lobe with an ON overshoot at longer latency (Fig. 3c). The ON overshoot of the centre and the ON surround together form a slanted feature in the space-time plane (Fig. 3b). A bright spot travelling in the preferred direction at the appropriate speed passes through both these regions, and the time delay of the centre produces superposition of the two excitations and an enhanced response[21]. This explains why an OFF-type neuron can be highly direction-selective for bright spots (Fig. 2e). Second, the OFF centre itself is also slanted in the space-time plane (Fig. 3b), which similarly renders dark spots more effective when moving in the preferred direction than when moving in the null direction. The space-time slope of the OFF centre, and thus the preferred speed for spot movement, is considerably greater than that of the slanted ON feature. Indeed, dark spots give the most direction-selective response at high speeds, whereas bright spots do so at low speeds (Supplementary Fig. 5).

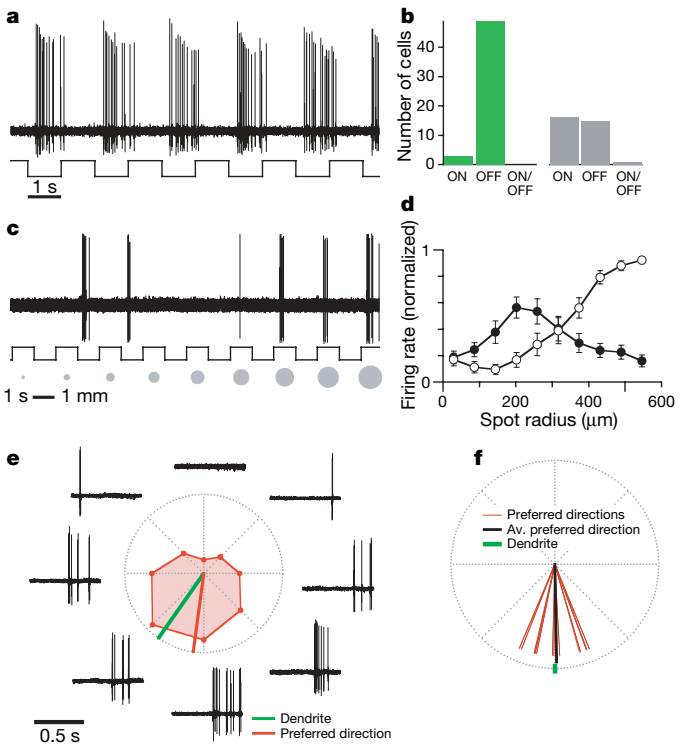

Figure 2 | J-RGCs are direction-selective OFF cells. **a**, Recording from a J-RGC during stimulation with a flashing spot 345 μm in diameter centred on the receptive field. **b**, Summary of response types encountered among 52 J-RGCs (green) and 32 YFP-negative RGCs probed with a flashing spot. **c**, Recording from a J-RGC with a flashing spot of increasing diameter. **d**, Average response of J-RGCs (means ± s.e.m., $n = 10$) to stimulus series in **c**. The graph shows number of spikes at light onset (ON response; open symbols) and offset (OFF response; filled symbols). **e**, Responses of a J-RGC to a small spot moving in directions indicated by dotted lines from the centre (white spot, 115 μm diameter, 575 μm s^{-1}; see Supplementary Fig. 5 for results with black spots). The average responses are displayed in a polar plot. The bold red line indicates the preferred direction, computed as the vector sum of the eight responses; the green line indicates the direction of the dendritic arbor. **f**, Relationship between dendritic asymmetry and direction selectivity of 12 J-RGCs. The preferred direction (computed as in **e**) is plotted relative to the direction of the dendritic arbor, arbitrarily shown as downward. The average preferred direction is indicated with the bold line.

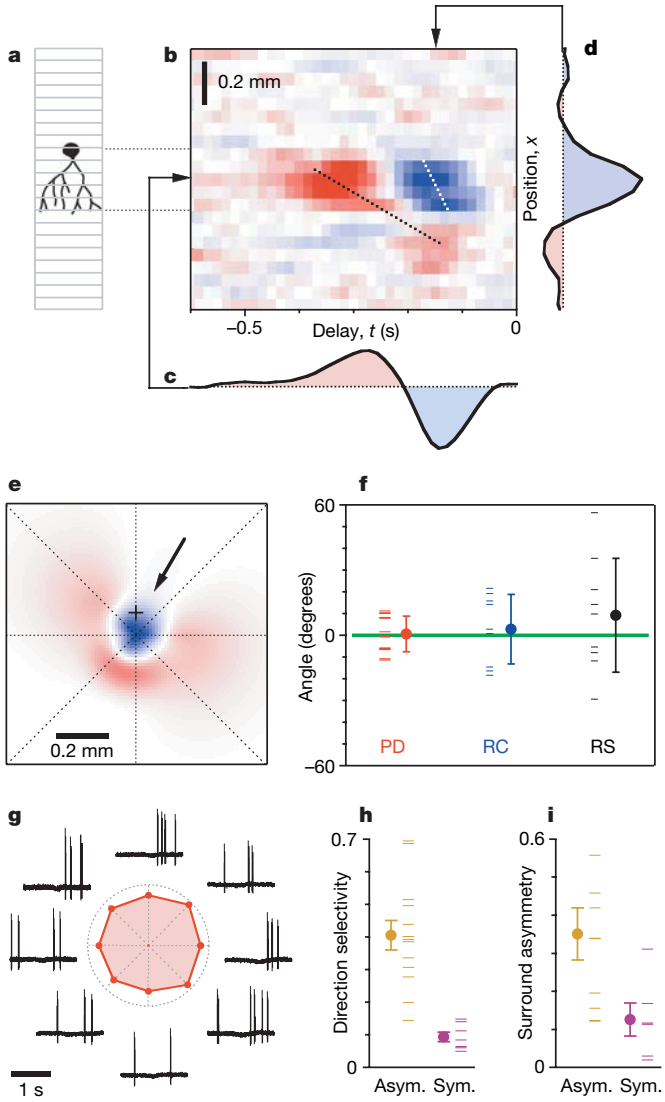

Figure 3 | Asymmetries in J-RGC receptive fields correspond to dendritic asymmetries. **a**, Measurement of receptive fields. The stimulus was a strip of narrow bars centred on the recorded cell. Each bar flickered randomly and independently of the others. **b**, Spatio-temporal receptive field $h(x,t)$ of one J-RGC, computed from responses to the stimulus of **a**. For a bar at position x (vertical axis), a row in this graph reports the average intensity that occurred at time t before a spike (horizontal axis): white, 0; red, positive; blue, negative. $h(x,t)$ approximates the firing rate elicited by a brief flash of light in bar x at time t. Two slanted features are indicated by dotted lines: one links the overshoot of the receptive field centre to the asymmetric surround (left); the other results from space-time slant within the receptive field centre itself (right). A moving bar that follows such a trajectory triggers many contributions from $h(x,t)$ that all have the same sign and thus elicit strong excitation. **c**, **d**, Time course (**c**) and spatial profile (**d**) of the receptive field at locations indicated by arrows. **e**, Two-dimensional spatial profile of the receptive field, obtained by interpolating data from four separate experiments with the grating strips (**a**) rotated at 45° increments. Arrow, preferred direction for spots; cross, location of cell body. **f**, Relation of functional asymmetries of J-RGCs to the direction of their dendrites (at 0°): the preferred direction for moving spots (PD), the direction of movement within the receptive field centre (RC), and the direction of displacement of the receptive field surround (RS). Lines, individual cells; circles, means ± s.d. **g**, Responses from a J-RGC with symmetrical dendrites at the ventral border of the retina, presented as in Fig. 2e. **h**, **i**, Direction selectivity and surround asymmetry of J-RGCs with asymmetrical and symmetrical dendrites. Direction selectivity is an index for asymmetry in the polar plot of moving spot responses (Fig. 2e). Surround asymmetry is an index for displacement of the ON surround relative to the OFF centre (**e**). Lines, individual cells; circles, means ± s.e.m.

In summary, J-RGCs show three functional asymmetries: the direction in which the receptive field surround is displaced (Fig. 3e), the space-time slant within the receptive field centre (Fig. 3b), and the preferred direction for spot movement (Fig. 2e). These three directions matched closely and coincided with the anatomical orientation of the dendritic arbor (Fig. 3f).

Does the direction selectivity of J-RGCs result from their structural asymmetry? To explore this relationship, we took advantage of the structurally symmetrical J-RGCs in ventral retina (Fig. 1i). These cells had no apparent preferred direction of movement and a relatively symmetrical ON surround (Fig. 3g–i). Moreover, across the entire J-RGC population, the degree of direction selectivity was correlated with the degree of asymmetry of the receptive field (Supplementary Fig. 6). Thus, within a single molecularly defined class of OFF-RGCs, dendritic structure and cell function are closely linked, suggesting that the latter arises from the former.

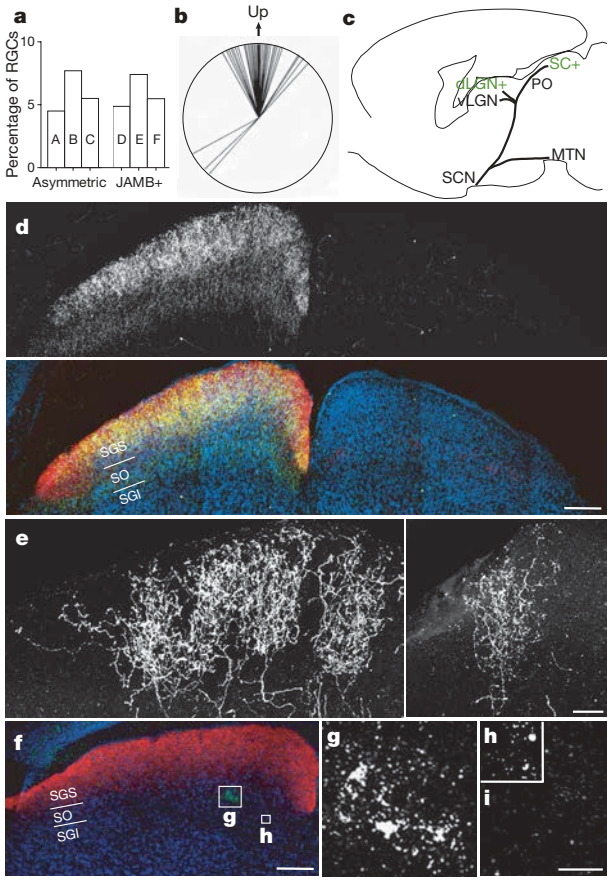

Figure 4 | Numbers and central projections of J-RGCs. **a**, The number of putative OFF RGCs with asymmetric morphology in mouse retina, reported in previous studies (A, RGC-C6 in ref. 14; B, type 6 in ref. 15; C, M5a in ref. 16) is similar to the number of J-RGCs estimated from JAM-B–CreER;Thy1-STOP–YFP double transgenic mice (D) or *in situ* hybridization (*JAM-B* cells/*Thy1*+ cells in E; *JAM-B* cells/Nissl^{+} cells in F, based on total cell number in ref. 30). **b**, Fig. 6 from ref. 24 (reproduced with permission of the American Physiological Society), showing preference of movement-sensitive cells in mouse superior colliculus for upward motion. **c**, Retinorecipient structures that were (green) or were not (black) innervated by J-RGCs, determined as in **d**. dLGN, dorsal lateral geniculate nucleus; vLGN, ventral LGN; MTN, medial temporal nucleus; PO, preoptic area; SC, superior colliculus; SCN, suprachiasmatic nucleus. **d**, Coronal section through superior colliculus of a JAM-B–CreER;Thy1-STOP–YFP mouse after monocular enucleation and cholera toxin injection. Top: axons of J-RGCs from the intact eye project to the SC. Bottom: overlay of J-RGC axons (green), all RGC axons (marked by cholera toxin, red) and cell bodies (blue). SGS, stratum griseum superficiale; SO, stratum opticum; SGI, stratum griseum intermedium. **e**, High-magnification views of J-RGC axons in superior colliculus. Left, group of arbors; right, single arbor. **f**, Coronal section through superior colliculus of a JAM-B–CreER;CAG-STOP–wheat-germ agglutinin (WGA) double-transgenic mouse. Enucleation and cholera toxin injection were as in **d**. **g–i**, WGA immunoreactivity in areas indicated by boxes in **f** (**g**, **h**) and in the opposite colliculus (**i**). Scale bars, 200 μm (**d**, **f**) and 50 μm (**e**, **g–i**).

Noting that J-RGCs point in a single direction, we considered the possibility that other asymmetric OFF RGCs point in other directions. We therefore compared the number of J-RGCs with the total number of RGCs with asymmetric dendrites in OFF sublaminae. Three previous catalogues of mouse RGCs[14–16] noted and named such cells. They were studied in sparsely labelled retinae, so the uniformity of their asymmetry was not realized, but it seems likely that they included J-RGCs. They comprised 5% of RGCs reconstructed in the three studies (40 out of 782; Fig. 4a). The fraction of RGCs that were *JAM-B*-positive was also about 5%, on the basis of *in situ* hybridization and YFP staining (Fig. 4a). The correspondence of these two numbers suggests that no sizable populations of OFF RGCs exist with asymmetric dendrites pointing in directions other than dorsal-to-ventral.

Where in the brain do J-RGCs send this directional information? We used YFP to trace the axons of J-RGCs. The entire retinal projection was labelled by injecting one eye with an anterograde tracer[22], allowing us to identify all retinorecipient nuclei (Fig. 4c)[22,23]. YFP-positive axons in these nuclei were of retinal origin, as shown by their absence after enucleation (Fig. 4d). J-RGCs projected most heavily to the superior colliculus (Fig. 4c–e), the major retinorecipient structure in mice[22]. Some J-RGCs also projected to the dorsal lateral geniculate nucleus. In contrast, we detected no J-RGCs in the pretectal nucleus, in the ventral nucleus of the lateral geniculate body or in the accessory optic system (Fig. 4c and Supplementary Fig. 7). The accessory optic system is a major site to which other direction-selective RGCs project[23].

The collicular termination of J-RGCs is intriguing in light of a study in which Dräger and Hubel mapped the receptive fields of neurons in the superior colliculus of the mouse[24]. Nearly all of the direction-selective neurons they studied (35 out of 38) preferred upward motion in the visual field (Fig. 4b). This preference corresponds to that of J-RGCs. Dräger and Hubel further noted that the highest densities of direction-selective cells in the colliculus were in two layers, the stratum opticum and intermediate grey layer[24]. To ask whether J-RGCs synapse on cells in these layers, we mated JAM-B–CreER mice to a transgenic line in which Cre-mediated recombination activates expression of the trans-synaptic tracer wheat-germ agglutinin[25]. Wheat-germ agglutinin immunoreactivity was detected in neurons of the stratum opticum and intermediate grey layer (Fig. 4f–i). We therefore propose that the receptive fields of direction-selective collicular cells are built from J-RGCs.

We have used a molecular strategy to identify J-RGCs, which differ in several respects from previously described direction-selective RGCs[4,5]. First, direction-selective OFF RGCs (Fig. 2a, b) have not previously been reported in mammals, although structurally asymmetrical orientation-selective RGCs present in rabbits[26] might be related to J-RGCs. Second, whereas no morphological feature predicted the preferred direction of previously described direction-selective RGCs, the orientation of the dendritic arbor is correlated with the preferred direction in J-RGCs (Figs 1h and 2f). Third, direction-selective ON and ON–OFF RGCs exist in multiple subclasses with distinct preferred directions[27], but direction-selective J-RGCs share a single preferred direction (Fig. 2f). Last, whereas the selectivity of other direction-selective RGCs depends on input from starburst amacrine cells, which themselves show directional responses[4,5], J-RGCs receive little input from these cells (Fig. 1e) and thus must rely on other mechanisms. One possible mechanism is suggested by the finding that inhibitory synapses on some RGCs are concentrated at distal dendrites[28]. Distal inhibition on the asymmetric dendrites of J-RGCs could account for their asymmetrically displaced surround.

One outstanding question is why the mouse has invested so heavily in sensitivity to upward motion. We have been no more successful than Dräger and Hubel[24] in guessing what that significance might be. By mating JAM-B–CreER mice to other transgenics bearing appropriate Cre-activated channels or toxins, we may be able to inactivate this pathway and thereby directly test its function.

METHODS SUMMARY

We obtained sequences of IgSF genes from public databases, and assessed their expression in postnatal retina by *in situ* hybridization[6,7] and RT–PCR. A construct in which regulatory sequences from the mouse *JAM-B* gene drove the expression of CreER was used to generate transgenic mice. These mice were mated to mice in which the expression of reporters[11,25] depended on Cre-mediated excision of STOP sequences. Staining protocols and antibodies used are detailed in Supplementary Methods.

To record visual responses from J-RGCs, we localized the cells by brief excitation (about 100–200 ms) with a blue light-emitting diode (LED) so they could be targeted with a cell-attached patch electrode. Light stimuli of photopic intensity were delivered by a computer-driven video projector.

Full Methods and any associated references are available in the online version of the paper at www.nature.com/nature.

Received 13 September; accepted 24 January 2008.

1. Masland, R. H. The fundamental plan of the retina. *Nature Neurosci.* **4,** 877–886 (2001).
2. Wässle, H. Parallel processing in the mammalian retina. *Nature Rev. Neurosci.* **5,** 747–757 (2004).
3. Nelson, R. & Kolb, H. in *The Visual Neurosciences* (eds Chalupa, L. M. & Werner, J. S.) 260–278 (MIT Press, Cambridge, MA, 2003).
4. Demb, J. B. Cellular mechanisms for direction selectivity in the retina. *Neuron* **55,** 179–186 (2007).
5. Taylor, W. R. & Vaney, D. I. New directions in retinal research. *Trends Neurosci.* **26,** 379–385 (2003).
6. Yamagata, M., Weiner, J. A. & Sanes, J. R. Sidekicks: synaptic adhesion molecules that promote lamina-specific connectivity in the retina. *Cell* **110,** 649–660 (2002).
7. Yamagata, M. & Sanes, J. R. Dscam and Sidekick proteins direct lamina-specific connections in vertebrate retina. *Nature* **451,** 465–469 (2008).
8. Rodieck, R. W. The density recovery profile: a method for the analysis of points in the plane applicable to retinal studies. *Vis. Neurosci.* **6,** 95–111 (1991).
9. Weber, C., Fraemohs, L. & Dejana, E. The role of junctional adhesion molecules in vascular inflammation. *Nature Rev. Immunol.* **7,** 467–477 (2007).
10. Branda, C. S. & Dymecki, S. M. Talking about a revolution: The impact of site-specific recombinases on genetic analyses in mice. *Dev. Cell* **6,** 7–28 (2004).
11. Buffelli, M. *et al.* Genetic evidence that relative synaptic efficacy biases the outcome of synaptic competition. *Nature* **424,** 430–434 (2003).
12. Roska, B. & Werblin, F. Vertical interactions across ten parallel, stacked representations in the mammalian retina. *Nature* **410,** 583–587 (2001).
13. Haverkamp, S. & Wässle, H. Immunocytochemical analysis of the mouse retina. *J. Comp. Neurol.* **14,** 1–23 (2000).
14. Sun, W., Li, N. & He, S. Large-scale morphological survey of mouse retinal ganglion cells. *J. Comp. Neurol.* **451,** 115–126 (2002).
15. Badea, T. C. & Nathans, J. Quantitative analysis of neuronal morphologies in the mouse retina visualized by using a genetically directed reporter. *J. Comp. Neurol.* **480,** 331–351 (2004).
16. Coombs, J., van der List, D., Wang, G. Y. & Chalupa, L. M. Morphological properties of mouse retinal ganglion cells. *Neuroscience* **140,** 123–136 (2006).
17. Fox, M. A. & Sanes, J. R. Synaptotagmin I and II are present in distinct subsets of central synapses. *J. Comp. Neurol.* **503,** 280–296 (2007).
18. Ghosh, K. K., Bujan, S., Haverkamp, S., Feigenspan, A. & Wässle, H. Types of bipolar cells in the mouse retina. *J. Comp. Neurol.* **469,** 70–82 (2004).
19. Croner, L. J. & Kaplan, E. Receptive fields of P and M ganglion cells across the primate retina. *Vision Res.* **35,** 7–24 (1995).
20. Chichilnisky, E. J. A simple white noise analysis of neuronal light responses. *Network* **12,** 199–213 (2001).
21. Barlow, H. B. & Levick, W. R. The mechanism of directionally selective units in rabbit's retina. *J. Physiol. (Lond.)* **178,** 477–504 (1965).
22. Ling, C., Schneider, G. E. & Jhaveri, S. Target-specific morphology of retinal axon arbors in the adult hamster. *Vis. Neurosci.* **15,** 559–579 (1998).
23. Giolli, R. A., Blanks, R. H. & Lui, F. The accessory optic system: basic organization with an update on connectivity, neurochemistry, and function. *Prog. Brain Res.* **151,** 407–440 (2005).
24. Dräger, U. C. & Hubel, D. H. Responses to visual stimulation and relationship between visual, auditory, and somatosensory inputs in mouse superior colliculus. *J. Neurophysiol.* **38,** 690–713 (1975).
25. Braz, J. M., Rico, B. & Basbaum, A. I. Transneuronal tracing of diverse CNS circuits by Cre- mediated induction of wheat germ agglutinin in transgenic mice. *Proc. Natl Acad. Sci. USA* **99,** 15148–15153 (2002).
26. Amthor, F. R., Takahashi, E. S. & Oyster, C. W. Morphologies of rabbit retinal ganglion cells with concentric receptive fields. *J. Comp. Neurol.* **280,** 72–96 (1989).
27. Oyster, C. W. & Barlow, H. B. Direction-selective units in rabbit retina: distribution of preferred directions. *Science* **155,** 841–842 (1967).
28. Lin, B., Martin, P. R., Solomon, S. G. & Grunert, U. Distribution of glycine receptor subunits on primate retinal ganglion cells: a quantitative analysis. *Eur. J. Neurosci.* **12,** 4155–4170 (2000).
29. Barnstable, C. J. & Dräger, U. C. Thy-1 antigen: a ganglion cell specific marker in rodent retina. *Neuroscience* **11,** 847–855 (1984).
30. Jeon, C. J., Strettoi, E. & Masland, R. H. The major cell populations of the mouse retina. *J. Neurosci.* **18,** 8936–8946 (1998).

Supplementary Information is linked to the online version of the paper at www.nature.com/nature.

Acknowledgements We thank S. Dymecki for FlpE mice, A. Basbaum for WGA mice and U. Dräger, S. Haddad, B. Howell, A. Koizumi, T. Kummer, J. Livet, D. Pelusi and E. Soucy for advice and assistance. This work was supported by grants from the National Institutes of Health to M.M. and J.R.S., a Merck Award and a Bushrod H. Campbell and Adah F. Hall Charity Fund Fellowship to I.J.K., and a Damon Runyon fellowship to Y.Z.

Author Contributions I.J.K., Y.Z., M.Y., M.M. and J.R.S. conceived the experiments. I.J.K and M.Y. performed molecular and histological experiments. Y.Z. performed physiological experiments. Y.Z. and M.M. performed computational analysis. M.M. and J.R.S. wrote the paper.

Author Information Reprints and permissions information is available at www.nature.com/reprints. Correspondence and requests for materials should be addressed to M.M. (meister@fas.harvard.edu) or J.R.S. (sanesj@mcb.harvard.edu).

METHODS

Identification of *JAM-B*-positive RGCs. We searched public databases for IgSF genes by using SMART (Simple Modular Architecture Research Tool; http://smart.embl-heidelberg.de). On the basis of sequences of other IgSF genes involved in synaptic recognition or differentiation, such as Sidekick-1 and Sidekick-2, SYG-1 and SYG-2, and SynCAM[6,7,31,32], we focused on the C2 family of Ig domains and on proteins with a carboxy-terminal PDZ domain-binding motif. We used RT–PCR to assess the expression of about 200 genes in P8 retinae; 161 genes were expressed. We then performed *in situ* hybridization on P7 and P18–P20 retina[6] to seek genes expressed in subsets of RGCs. In brief, riboprobes were synthesized with either digoxigenin-labelled or fluorescein-labelled UTP and detected by anti-digoxigenin or anti-fluorescein antibodies conjugated to alkaline phosphatase[6]. For double labelling, peroxidase-conjugated antibodies were used and signals were detected with a tyramide signal amplification system (TSA-Plus system; Perkin-Elmer Life Sciences).

Transgenic marking of *JAM-B*-positive RGCs. A bacterial artificial chromosome (BAC) containing the mouse *JAM-B* gene was obtained from Children's Hospital Research Institute. Using homologous recombination in bacteria[33], we first removed the *loxP* site and sufficient genomic sequence from the vector to leave about 80 kb of BAC. We then introduced a cassette that included *Cre-ER*, a polyadenylation signal, and a neomycin resistance gene flanked by *frt* sites (*frt-neo-frt*), replacing the translational start site of *JAM-B* with that of *Cre-ER*. Homology arms from the *JAM-B* gene for this step were amplified from the BAC by using the following primers: 5′-ACCCTTCA-AAAGAAGGACTGTCCC-3′ and 5′-CTACGCGGGCGCCAGCTGGCTG-3′ for the 5′ homology arm, and 5′- ACACTACTTGATCGTCGCCCTG-3′ and 5′- TACAAGACGCACAGGACTTCAGTC-3′ for the 3′ homology arm. DNA was injected into fertilized oocytes by standard techniques to generate transgenic mice. The *Neo* cassette was then removed by mating transgenics to mice that express FLP recombinase ubiquitously[34]. These mice were then mated to Thy1-STOP–YFP transgenic mice, which have been described previously[12]. To activate Cre and thereby YFP, tamoxifen (100 μg, dissolved in corn oil at 20 mg ml^{-1}; T5648; Sigma) was injected intraperitoneally at P0 and/or P1.

Histology. Mice were killed by intraperitoneal injection of Nembutal and perfused with 4% paraformaldehyde (PFA) in PBS. Retinae were dissected out, fixed for 1 h in 4% PFA/PBS, incubated for 2 h with 30% sucrose/PBS, frozen, and then sectioned at 20 μm in a cryostat. Sections were treated successively with 0.1% Triton X-100/PBS and blocked with 3% donkey serum/0.1% Triton X-100/PBS for 30 min each at 20–22 °C, then incubated successively with primary antibodies overnight at 4 °C and with secondary antibodies for 2 h at room temperature. For whole mounts, retinae were kept in 4% PFA/PBS for 2 h and washed with PBS before being stained.

Antibodies used were as follows: rabbit anti-GFP (dilution 1:2,000, Ab3080P; Chemicon), chick anti-GFP (dilution 1:500, GFP-1020; Aves Labs), goat anti-choline acetyltransferase (dilution 1:250, AB144P; Chemicon), goat anti-vesicular acetylcholine transporter (dilution 1:1,000, G488A; Promega), rabbit anti-tyrosine hydroxylase (dilution 1:500, AB152; Chemicon), mouse anti-synaptotagmin 2 (dilution 1:200, ZNP-1; Zebrafish International Resource Center), rabbit anti-Disabled-1 (dilution 1:500; ref. 35), mouse anti-CD15 antibody (dilution 1:50, DSHB), rabbit anti-recoverin (dilution 1:4,000, 55A5; Chemicon), rabbit anti-neurokinin receptor 3 (dilution 1:5,000, 480739; Calbiochem), mouse anti-protein kinase C (dilution 1:500, MC5; ABCAM) and goat anti-Gγ13 (dilution 1:200, SC26781; Santa Cruz). Secondary Alexa Fluor 488- and 568- conjugated antibodies (Invitrogen) were diluted 1:500. For previously described staining patterns with these antibodies, see refs 14, 18, 19, 35, 36.

Brains were post-fixed overnight in 4% PFA/PBS at 4 °C, then either incubated overnight with 30% sucrose/PBS, frozen and sectioned at 30 μm in a cryostat or washed in PBS, mounted in a Vibratome and sectioned at 55 μm. To facilitate the detection of wheat-germ agglutinin we preabsorbed rabbit anti-wheat-germ agglutinin (3 μg ml^{-1}, T4144; Sigma) with 1% acetone powder of mouse brain, included 0.5% Triton X-100 in antibody solutions, treated sections with Image-iT FX signal enhancer (I36933; Invitrogen), and diluted secondary antibody (dilution 1:500, donkey anti-rabbit Cy3 conjugated; Jackson ImmunoResearch) in Renoir Red (PD904L; Biocare Medical). In some cases, immunohistochemistry was combined with *in situ* hybridization, as described in ref. 6.

For injection of cholera toxin B subunit (CTB), mice were anaesthetized by intraperitoneal injection of ketamine/xylene (1.7 mg/20 g). CTB conjugated to Alexa Fluor 488 or Alexa Fluor 594 (1–2 μl of 1 mg ml^{-1} solution, C-22841 or C-22842; Invitrogen) was injected into one eye with a 33-gauge custom-made needle (1.5 inches long, type no 4, 30° of bevel, 7803-05; Hamilton).

Recording. The dark-adapted mouse retina was isolated under an infrared microscope into oxygenated Ringer's solution (110 mM NaCl, 2.5 mM KCl, 1 mM $CaCl_2$, 1.6 mM $MgCl_2$, 22 mM $NaHCO_3$ with constant bubbling of 95% O_2, 5% CO_2) at room temperature. A piece of retina, about 3–4 mm on a side, was placed with ganglion cells facing upwards in a superfusion chamber on the stage of an upright fluorescence microscope. Patch microelectrodes were filled with Ringer's medium and had a final impedance of 5–8 MΩ. Fluorescent J-RGCs were detected by brief excitation (about 100–200 ms) with a blue LED, to minimize photobleaching. To ensure that recorded cells were J-RGCs, we applied gentle suction until a small YFP-positive protrusion was pulled into the recording pipette. Once recording was complete, we revealed the cells with more intense fluorescence illumination, and photographed the dendritic arbor. The orientation of the arbor was estimated as the midpoint of the angular sector occupied by the principal dendrites.

Stimulation. Light stimuli were delivered from a computer-driven video projector through a custom-made substage lens system and focused onto the photoreceptors (frame rate 60 Hz, magnification 5.75 μm/pixel). White light was used, and the average intensity for both flashing spots and flickering bars was equivalent to the following photon flux values for the three mouse photoreceptors: rod, 6.7×10^4 photons s^{-1} cm^{-2} at $\lambda_{max} = 500$ nm; M cone, 8.2×10^4 photons s^{-1} cm^{-2} at $\lambda_{max} = 511$ nm; S cone, 1.2×10^3 photons s^{-1} cm^{-2} at $\lambda_{max} = 370$ nm. For comparison the respective values for the blue LED used for brief fluorescence imaging were 6.8×10^7, 5.6×10^7 and 6.8×10^5 photons s^{-1} cm^{-2}.

After patching onto a RGC, a flashing spot stimulus was centred on the soma to test the neuron's response type. The few J-RGCs recorded as having ON responses (Fig. 2b) may be OFF cells inadvertently stimulated with a slightly misaligned spot. To map the receptive field, we projected gratings of adjacent thin bars (58 μm width) as in Fig. 3a. In each bar, the intensity flickered black or white according to a pseudo-random binary sequence (67 ms frame duration)[37]; in some experiments a chequerboard of square tiles was used instead. Moving spot stimuli consisted of a white or black square (width 115 μm) on a grey background moved through the receptive field centre in eight different directions consecutively, with a 0.5-s pause between sweeps. The total distance traversed by the spot varied from 575 μm to 2,300 μm, and was always centred on the receptive field centre. The speed of movement varied from 288 μm s^{-1} to 575 μm s^{-1}, except in Supplementary Fig. 5, in which values up to 2,880 μm s^{-1} were explored.

Analysis. The response to flashing spots (Fig. 2d) was quantified by counting spikes in the interval between 0.1 s and 1 s after the onset or the offset of the flash, and normalizing to the maximum value obtained. The resulting relative response strength was then averaged across cells.

To quantify the response to a moving spot, we smoothed the spike train (gaussian filter, s.d. 60 ms), averaged the resulting function over several trials with identical sweeps of the spot, and computed the standard deviation of this firing rate throughout the trial. This number was taken as the response amplitude $r(\varphi)$, where φ is the direction of the moving spot (Figs 2e and 3g). From experiments with eight directions, $\varphi_k = 0°, 45°, 90°, 135°, 180°, 225°, 270°$ and $315°$, the preferred direction φ_P (Figs 2e, f and 3f, g) was computed as the angle of the vector sum in a polar plot of responses:

$$\varphi_P = \arg \sum_k r(\varphi_k) e^{i\varphi_k} \quad (1)$$

We also computed an index for direction-selectivity:

$$D = \left| \sum_k r(\varphi_k) e^{i\varphi_k} \right| \Big/ \sum_k r(\varphi_k) \quad (2)$$

This corresponds to the length of the vector sum, divided by the sum of all responses. It ranges from 0 for a cell with equal response in all directions to 1 for a cell that responds to only one direction (Fig. 3h and Supplementary Fig. 5b).

The spatio-temporal receptive field $h(x,t)$ was computed as the spike-triggered average of the flickering bar stimulus (Fig. 3b–d). If $s(x,t)$ is the stimulus intensity at location x and time t, with the time-averaged intensity subtracted, and the neuron fires at spike times $\{t_j\}$, then

$$h(x,t) = \frac{1}{n} \sum_{j=1}^{n} s(x, t_j + t) \quad (3)$$

To derive a two-dimensional receptive field profile (Fig. 3e), we performed four experiments with strips of bars (Fig. 3a) rotated in 45° increments. In each case, we computed a one-dimensional profile at the time point with the strongest antagonistic surround (as in Fig. 3d). Then the four profiles were plotted on a common graph and intervening points were estimated by interpolation. We attempted the more straightforward approach using a two-dimensional checkerboard[37], but found that this stimulus strongly inhibits the J-RGCs, presumably

because it activates a suppressive surround mechanism. By comparison, the one-dimensional grating strips stimulate the surround only in a narrow strip.

The direction of movement within the receptive field centre (Fig. 3f) was again estimated from four grating experiments. For each of the four grating directions $\vartheta_k = 0^\circ$, 45°, 90° and 135° we computed the spatial profile of the receptive field $h(x,t)$ as in Fig. 3d. The large negative lobe of this curve was taken as the receptive field centre. We computed the location of the centre of mass of this lobe at various times t, and from that the average speed $v(\vartheta_k)$ at which the centre moved. The direction of this movement was obtained by a vector average over the four experiments:

$$\varphi_C = \arg \sum_k v(\vartheta_k) e^{i\vartheta_k} \quad (4)$$

The velocity of movement in the receptive field centre was taken as

$$v_C = \frac{1}{2} \left| \sum_k v(\vartheta_k) e^{i\vartheta_k} \right| \quad (5)$$

The asymmetry of the surround (Fig. 3f, i) was evaluated in a similar fashion starting from the linear spatial profile (Fig. 3d). This profile was fitted by a difference-of-gaussians curve. The positive lobes on either side of the negative centre were taken as the surround. On each side of the centre, we computed the relative strength of the surround as

$$s = \int_x h_S(x)\,dx \Big/ \int_x h_C(x)\,dx \quad (6)$$

where $h_S(x)$ is the surround lobe and $h_C(x)$ the centre lobe. This resulted in values of the surround strength $s(\varphi_k)$ in eight different directions φ_k from the centre. We averaged the result over several time points t at which the surround was prominent. Finally, the direction of displacement of the surround (Fig. 3f) was obtained from the vector average

$$\varphi_S = \arg \sum_k s(\varphi_k) e^{i\varphi_k} \quad (7)$$

and the strength of the surround asymmetry (Fig. 3i) from

$$A = \left| \sum_k s(\varphi_k) e^{i\varphi_k} \right| \quad (8)$$

The relationship between the degree of direction selectivity, surround asymmetry and centre velocity is illustrated in Supplementary Fig. 6.

The direction of the dendritic arbors was computed in whole-mount micrographs. For each cell we drew the convex polygon linking the soma and dendritic tips, then computed the vector from the soma to the centre of mass of the polygon. During online recording experiments, the fluorescence optics did not reveal the finest dendritic tips, but the direction of the arbor could be obtained reliably from following the principal dendrites.

31. Biederer, T. *et al.* SynCAM, a synaptic adhesion molecule that drives synapse assembly. *Science* **297,** 1525–1531 (2002).
32. Shen, K., Fetter, R. D. & Bargmann, C. I. Synaptic specificity is generated by the synaptic guidepost protein SYG-2 and its receptor, SYG-1. *Cell* **116,** 869–881 (2004).
33. Lee, E. C. *et al.* A highly efficient *Escherichia coli*-based chromosome engineering system adapted for recombinogenic targeting and subcloning of BAC DNA. *Genomics* **73,** 56–65 (2001).
34. Farley, F. W., Soriano, P., Steffen, L. S. & Dymecki, S. M. Widespread recombinase expression using FLPeR (flipper) mice. *Genesis* **28,** 106–110 (2000).
35. Rice, D. S. & Curran, T. Disabled-1 is expressed in type AII amacrine cells in the mouse retina. *J. Comp. Neurol.* **424,** 327–338 (2000).
36. Jakobs, T. C., Ben, Y. & Masland, R. H. CD15 immunoreactive amacrine cells in the mouse retina. *J. Comp. Neurol.* **465,** 361–371 (2003).
37. Meister, M., Pine, J. & Baylor, D. A. Multi-neuronal signals from the retina: acquisition and analysis. *J. Neurosci. Methods* **51,** 95–106 (1994).

doi: 10.1038/nature06739

MOLECULAR IDENTIFICATION OF A NOVEL RETINAL CELL TYPE THAT RESPONDS TO UPWARD MOTION

In-Jung Kim, Yifeng Zhang, Masahito Yamagata, Markus Meister and Joshua R. Sanes
Department of Molecular and Cellular Biology and Center for Brain Science
Harvard University, Cambridge MA, 02138, USA

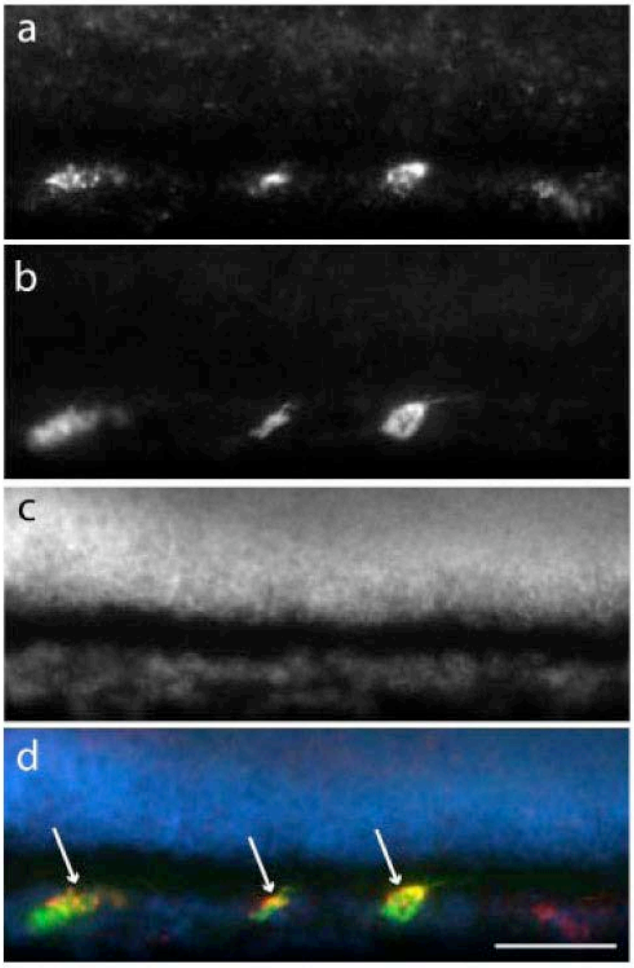

Supplementary Figure 1. Section of JAM-B-CreER;Thy1-STOP-YFP double transgenic retina probed by in situ hybridization for *JAM-B* (**a**) and by immunostaining for YFP (**b**). **c.** DAPI (nuclear) stain. **d.** Merge. Bar is 50 μm.

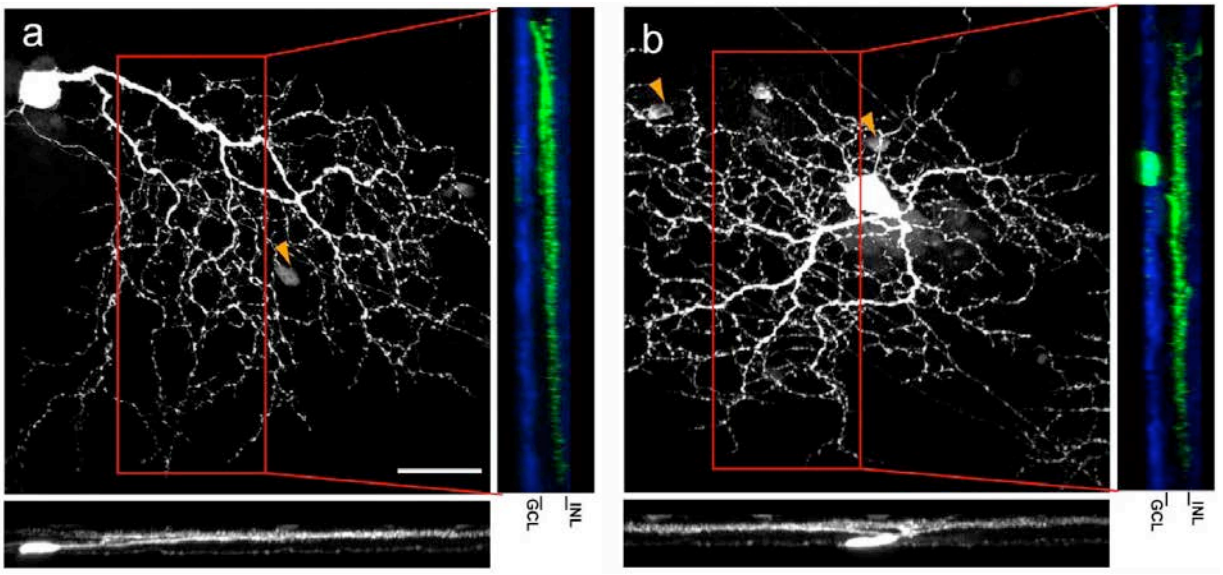

Supplementary Figure 2. Confocal reconstructions of an asymmetrical J-RGC near the center of a retina (**a**) and a symmetrical J-RGC near the ventral margin of the retina (**b**). Ninety degree rotations of the image stacks (boxed region at right and whole image at bottom) show that dendrites of both asymmetrical and symmetrical J-RGCs arborize in the outer portion of the IPL. Previously described ON- and ON-OFF direction-selective mouse ganglion cells[38,39] differ from those described here: their dendrites are less asymmetrical and arborize in different IPL sublaminae. Some amacrine cells also expressed YFP in JAM-B-CreER;Thy1-STOP-YFP double transgenic mice (arrowheads in **b**; see also show Figs. 1e and Supplementary Fig. 3e), but these cells expressed little if any endogenous *JAM-B*, as assessed by in situ hybridization. We suspect their labeling reflects ectopic expression of CreER from the transgene. Scale bar is 50 μm.

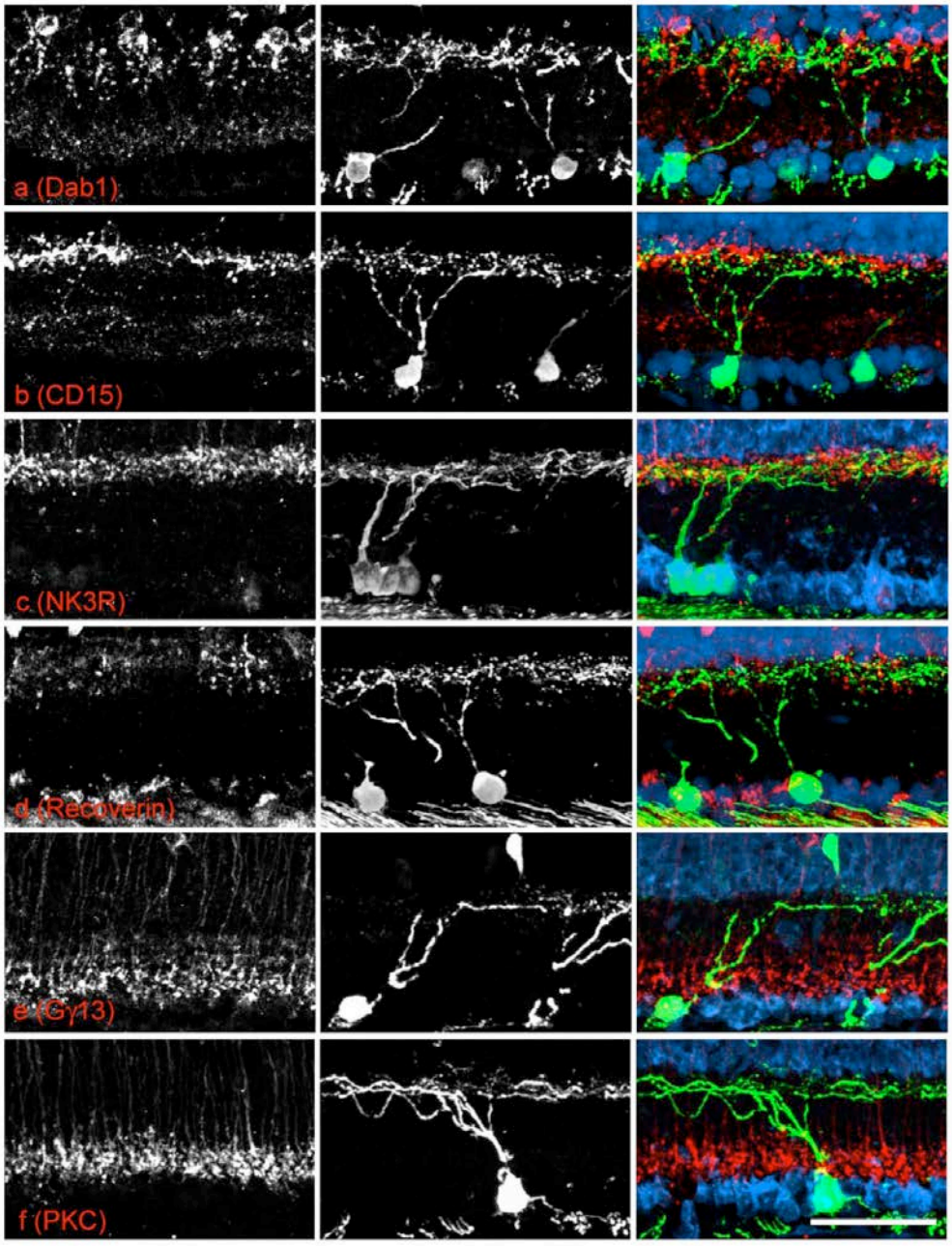

Supplementary Figure 3. Sections of retinae from JAM-B-CreER;Thy1-STOP-YFP mice were double labeled with antibodies to GFP (middle panels and green in right panels) and cell type-specific markers (left panels and red in right panels). **a.** Dab1 labels type IIA amacrines[35]. **b.** CD15 labels a subset of amacrines known to arborize near the inner nuclear layer[36]. **c.** Neurokinin-3 receptor marks OFF bipolar type 1 and 2 cells. **d.** Recoverin labels type 2 OFF bipolar cells. **e.** Gγ13 labels ON bipolar cells. **f.** PKC marks ON rod bipolar cells. Scale bar is 50 μm.

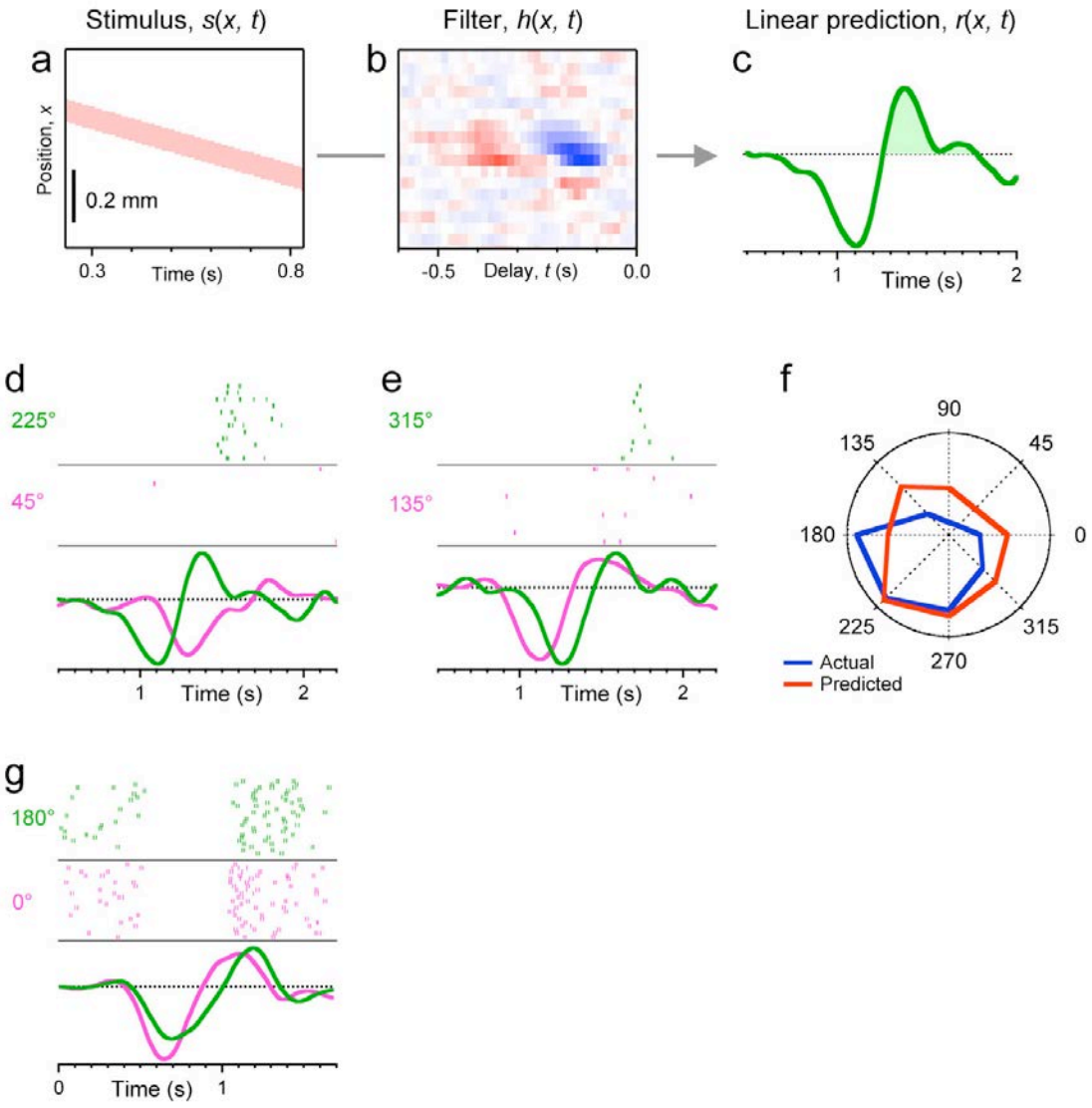

Supplementary Figure 4. Linear model of the ganglion cell response to moving spots. **a.** Space-time diagram $s(x,t)$ of a 115-μm wide bright spot moving in the x-direction at 575 μm/s. **b.** Spatio-temporal receptive field $h(x,t)$ of a J-RGC, computed from a strip of flickering bars along the same direction (see Fig 3a, b). **c.** In a linear approximation of the neuron's behavior[20], the time-reverse of the receptive field, $h(x,-t)$ can be interpreted as the impulse response of the cell's firing rate to a brief flash at position *x* and time *t*. Thus a linear prediction $r(x,t)$ of the

response to the moving spot is obtained by convolving $s(x,t)$ with $h(x,-t)$: $r(x,t) = \iint_{x\ t'} s(x,t') \cdot h(x,t'-t)\,dt'dx$. The initial negative overshoot occurs when the bright spot enters the cell's OFF receptive field center. The subsequent positive peak results when the spot leaves the OFF center and enters the ON surround. To predict the cell's firing rate, which is necessarily positive, this linear response must be rectified by some non-linear transform, such as the half-wave rectification illustrated by the shaded portion. **d.** Comparison of the measured spike trains obtained from two opposite directions of spot motion (raster graphs of multiple trials at top and middle) with the predicted responses $r(x,t)$ (bottom). For one direction (225°) the prediction makes a large positive excursion, and indeed the neuron fires many spikes; for the opposite direction (45°) the prediction barely crosses into positive values, and only few spikes are observed. **e.** As in panel d, for the orthogonal directions of motion. Here the predicted response is almost equally large for both directions, and indeed they produce similar spike numbers. Note $r(x,t)$ predicts that the response to 135° should begin earlier than to 315°, and indeed this occurs in the actual spike trains. **f.** Actual and predicted response of this J-RGC to the 8 directions. We performed this analysis on 6 J-RGCs for which all the required experiments could be performed. In each case we computed the preferred direction from the actual and the predicted responses, as described in Methods. The average discrepancy between the actual preferred direction and that predicted from a linear model was 47°. **g.** Comparison of measured spike trains and predicted responses to two opposite directions for a symmetric J-RGC. This neuron had a maintained firing rate at rest, which better illustrates the correspondence between actual and predicted responses. The initial negative transient in the prediction is matched by a sharp suppression of firing. The subsequent positive lobe of the prediction corresponds to a sharp increase in firing, which then declines back to the resting level. Note the predicted response peak for 0° occurs earlier than for 180°, and this is also observed in the actual response.

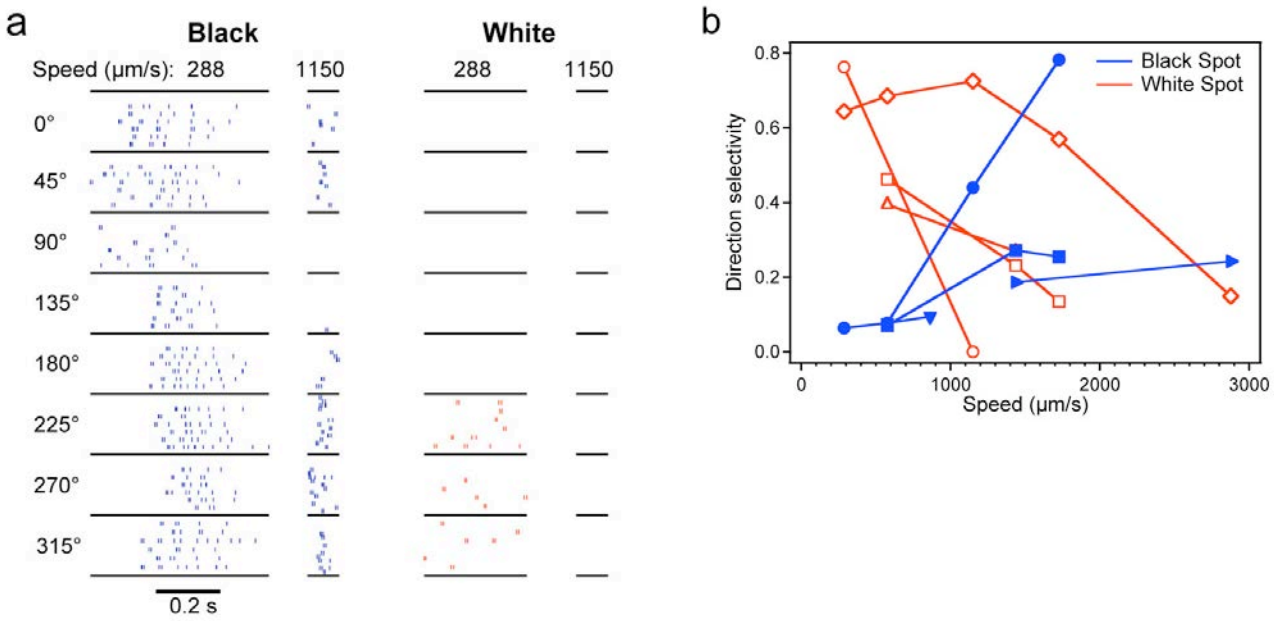

Supplementary Figure 5. Responses to black and white spots at different speeds. **a.** Sample responses from one J-RGC to spots moving in 8 different directions. The spot was either black (left) or white (right), and moved at low speed (288 μm/s) or high speed (1150 μm/s). For each condition, spike trains from several trials are shown in a raster plot. At low speed, the spot takes longer to traverse the receptive field, and thus the period of firing is longer as well. Note that the response to the black spot was more direction-selective at high speeds than at low speeds. By contrast, the response to the white spot was direction-selective at low speeds and failed entirely at high speeds. The preferred direction was almost identical under all conditions. **b.** Direction selectivity index (see Fig. 3h and Methods) obtained using white spots (open symbols) and black spots (closed symbols) at various speeds. Results from 6 J-RGCs denoted with different symbol shapes. Note that the response is more direction-selective at low speeds with white spots, but at high speeds with black spots. This accords with predictions derived from the spatio-temporal receptive field (Fig. 3b).

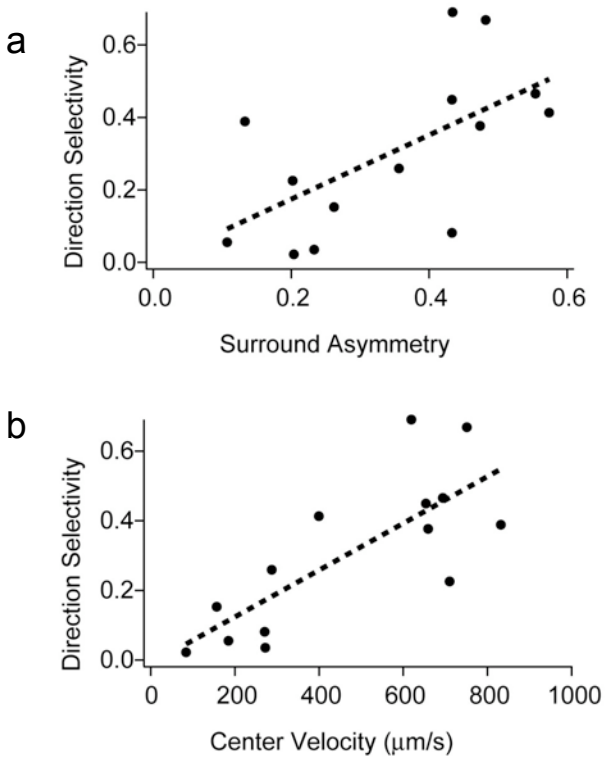

Supplementary Figure 6. Correlations between three measures of functional asymmetry in the population of J-RGCs. The strength of direction selectivity to moving spots (D , Eqn 2) is plotted against the degree of surround asymmetry (A , Eqn 8) in panel **a** and the spatio-temporal slope in the receptive field center (v_c , Eqn 5) in panel **b**. Pearson's coefficient (r) of correlation and Kendall rank correlation coefficient (τ) are r=0.62 ($p<0.02$), τ =0.47 ($p<0.02$) for **a** and r=0.77 ($p=0.001$) and τ =0.52 ($p=0.01$) for **b**.

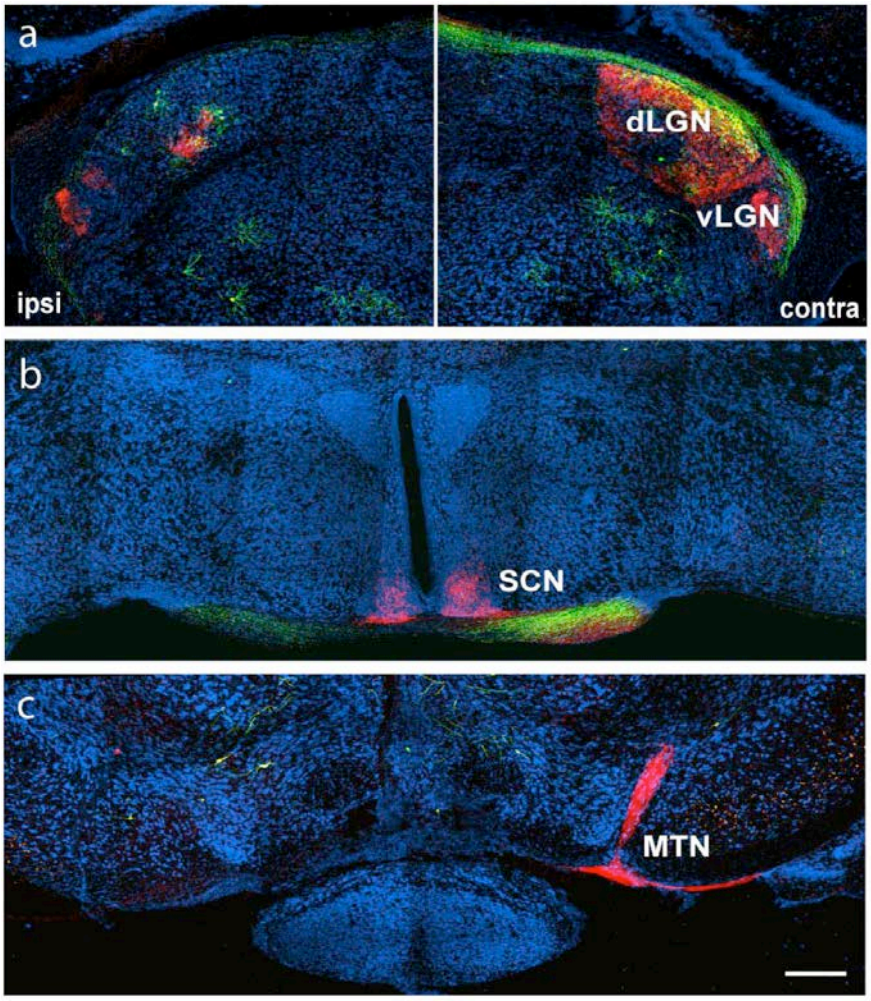

Supplementary Figure 7. Axonal arborizations of J-RGCs in the brain. Vibratome sections from JAM-B-CreER;Thy1-STOP-YFP mice were immunostained with anti-GFP. Axons of J-RGCs (green) terminate in dorsal lateral geniculate nucleus (dLGN; **a**) but not in ventral LGN (vLGN; **a**), suprachiasmatic nucleus (SCN; **b**), or medial temporal nucleus (MTN; **c**). All RGC axons were labeled by cholera toxin (red). One eye was removed 1 month before sacrifice. Scale bar is 250 μm.